

Development of a QMC code to tackle interacting electronic systems in 2D with application to TMD nanoribbons

Francisco Monteiro de Oliveira Brito
francisco.brito@tecnico.ulisboa.pt

Instituto Superior Técnico, Lisboa, Portugal

October 2018

Abstract

The discovery of two-dimensional materials, has renewed interest in the many-electron problem since electron-electron interactions play an important role in the description of many of the properties of these systems. Moreover, the rapid increase in computational power, and algorithmic sophistication in the last few decades has made it possible to attack many problems in the field that were previously intractable. In this work, we focus on emerging edge-state magnetism in Transition Metal Dichalcogenides nanoribbons. We consider a recently introduced symmetry-based tight-binding model, found to capture edge state-related properties of the system, and we generalize it to interacting case by considering intra-orbital Hubbard-type interactions. Our approach to this problem is two-fold. We start by performing original numerical mean field calculations and build an approximate physical picture of the system at hand. Then, we use our own implementation of the unbiased, state-of-the-art Determinant Quantum Monte Carlo algorithm to simulate this interacting, quantum many-fermion system.

Keywords: Two-dimensional Materials, Hubbard Model, Strongly Correlated Electrons, Transition Metal Dichalcogenide Nanoribbons, Mean Field Theory, Determinant or Auxiliary Field Quantum Monte Carlo

1. Introduction

Planar materials have steadily been drawing the attention of the community since graphene was isolated from a graphite sample by mechanical exfoliation [1]. In fact, in spite of its undeniable potential both from a fundamental and an application point of view, graphene has some shortcomings. This motivated the community to study other more complex graphene-like materials, which could have other desirable properties, while maintaining most of graphene's potential.

Transition Metal Dichalcogenides (TMDs) are a class of such materials, appearing in the form of a variety of nanostructures. Unlike in graphene, where the effects of electron interactions are relatively weak, in TMDs, electrons are strongly correlated, and one cannot overlook the interactions between them. In strongly correlated electron systems, the complexity created by the interactions among all constituents of the system gives rise to emergent phenomena. The properties of the system's components do not directly percolate up; instead, they shape the interactions that dictate the system's properties sometimes in rather unexpected ways, leading to unusual behavior. Analytical ap-

proaches to the solution of the problem are either hopeless, or rely on possibly unrealistic approximations. In fact, the increased complexity of the models describing such highly correlated materials, compared to their graphene counterparts, calls for sophisticated computer simulation methods, most notably Quantum Monte Carlo (QMC).

Much like graphite which is essentially constituted by stacked monolayers of carbon atoms bound by weak Van der Waals forces, 3D TMD structures are also formed by weakly bound layers. However, instead of carbon, the layers contain transition metals M , and chalcogens X , in a 1 – 2 proportion. Thus, group 6 TMD are denoted MX_2 , where $M = \text{Mo, W, ...}$ (respectively Molybdenum and Tungsten) and $X = \text{S, Se, Te}$ (respectively Sulfur, Selenium and Tellurium). Each TMD monolayer contains a layer of M atoms organized in a triangular lattice sandwiched between two layers of X atoms, unlike graphene.

Each M atom is coordinated with six X atoms, in a stacked structure with various possible coordinations for the X atoms. The most common phases are trigonal prismatic (2H) and octahedral (1T), typically in the few Å range (for Molybdenum disul-

fide, MoS₂, the width is around 6.5 Å). Here we will consider the 2H configuration, whose planar honeycomb lattice is depicted in the top-down view of Fig (1a). The valence bands arise out of the hybridization of the d_{xy} and $d_{x^2-y^2}$ orbitals of the transition metal with the $p_{x,y}$ orbitals of the chalcogen, while conduction bands have a main contribution from the $d_{3z^2-r^2}$ orbitals of the M atoms with only a minor contribution from the $p_{x,y}$ orbitals of the X atoms.

2. Background

In this section we summarize the main aspects of the three most important parts of this work: the tight-binding model used to describe TMD nanoribbons, and its extension to the interacting case via on-site intra-orbital interactions; the mean field theory of this model, and the iterative solution of the corresponding self-consistent equation; the simulation of the model using Determinant Quantum Monte Carlo.

2.1. Minimal 3-band tight-binding model

Here, we present a minimal model describing the low energy physics of group 6 TMD monolayers [2]. To obtain this tight-binding model, one uses the symmetries of the monolayer, and the fact that at low energies, both band edges have major contributions from d_{z^2} , d_{xy} , and $d_{x^2-y^2}$ orbitals of M-atoms and the p -orbitals of the X-atoms (which contribute very little at the band edges). This is illustrated for MoS₂ in Fig.(2). Near the Fermi energy, the Mo d -orbitals are clearly more populated at the K point (circled in orange), hence these atomic orbitals contribute more to the Bloch states near that point.

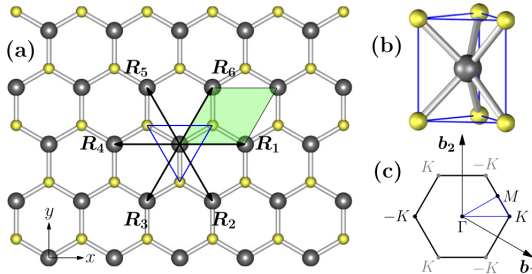


Figure 1: (a) The 2H phase of a TMD monolayer may be viewed simply as a $M - X$ honeycomb lattice. Here we represent the six nearest neighbors of a point on the M triangular lattice by the real space vectors $\mathbf{R}_{i=1,2,\dots,6}$. (b) Unit cell of the trigonal prismatic (2H) phase of a TMD monolayer. (c) High symmetry points Γ, M, K of the first Brillouin zone ($\mathbf{b}_{1,2}$ are the reciprocal basis vectors. (taken from [2]).

The existence of mirror symmetry through the $x - y$ plane (see Fig.(1b)) imposes that no hy-

bridization can occur between the sets of orbitals $\{d_{z^2}, d_{xy}, d_{x^2-y^2}\}$ and $\{d_{xz}, d_{yz}\}$ (d_{yz} and d_{xz} orbitals are not symmetric under reflection upon the $x - y$ plane). At low energies, the former are known to be the most relevant for the band structure of TMDs (see Fig.(2)). These considerations motivate us to construct a three-band tight-binding model.

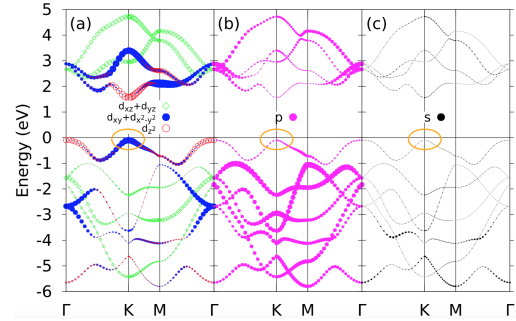


Figure 2: Orbital projected band structures for monolayer MoS₂ obtained from first principles. The Fermi energy is set to 0, and the symbol size is proportional to the population of the state. The panels represent the contributions from: (a) Mo d -orbitals; (b) All p -orbitals, dominated by S atoms; (c) All s -orbitals.

Moreover, the remaining point-symmetry operations impose a constraint on the number of independent hopping parameters. By fitting to first principles results obtained from density functional theory for the materials' energy bands, the hopping parameters can be obtained. The strategy that is chosen to do the fit in [2] is to fit the band energies at the high-symmetry \mathbf{k} -points Γ , K , and M , and the energies of the valence and conduction bands near K by least-squares. This procedure leads to a non-uniform nearest neighbor (NN) hopping matrix on the M-atom triangular lattice. Note that since the argument is purely based on symmetry, in general, the $d - d$ hoppings include both direct $d - d$ interactions of M atoms, and indirect ones, mediated by $X - p$ orbitals. These M-M hoppings suffice to describe the band-edge properties near the $\pm K$ valleys. By including third nearest neighbor hoppings, one can reproduce the energy dispersion in the entire first Brillouin zone. We consider a “spinless” model. Let the greek indices represent orbital space, except for σ , meaning spin. Then, the tight-binding Hamiltonian reads

$$\mathcal{H} = \sum_{i,j,\sigma} \sum_{\alpha,\beta} c_{i,\alpha}^\dagger t_{\alpha\beta}^\sigma (\mathbf{R}_i - \mathbf{R}_j) c_{j,\beta} + t_{\alpha\beta}^\dagger(\mathbf{R}) = t_{\alpha\beta}^\dagger(\mathbf{R}) \quad (1)$$

where we consider the basis set $\{|\alpha\rangle\}_{\alpha=1}^3 =$

$\{(d_{z^2}), (d_{xy}, d_{x^2-y^2})\}$. Let

$$\begin{aligned}\varepsilon_1 &= t_{11}^{11}(\mathbf{0}) \quad \varepsilon_2 = t_{22}^{11}(\mathbf{0}) = t_{22}^{22}(\mathbf{0}) \\ t_0 &= t_{11}^{11}(\mathbf{R}_1) \quad t_1 = t_{11}^{12}(\mathbf{R}_1) \quad t_2 = t_{12}^{12}(\mathbf{R}_1) \\ t_{11} &= t_{11}^{22}(\mathbf{R}_1) \quad t_{12} = t_{12}^{22}(\mathbf{R}_1) \quad t_{22} = t_{22}^{22}(\mathbf{R}_1)\end{aligned}$$

The on-site energies ε_j corresponding to the atomic orbitals $|\phi_\mu^j\rangle$ appear through a diagonal

$$\mathbf{t}(\mathbf{R}_{2,5(3,6)}) \equiv \mathbf{t}^{2,5(3,6)} = \begin{pmatrix} t_0 & \pm \left(\pm \frac{1}{2}t_1 - \frac{\sqrt{3}}{2}t_2 \right) & \mp \frac{\sqrt{3}}{2}t_1 - \frac{1}{2}t_2 \\ \pm \left(\mp \frac{1}{2}t_1 - \frac{\sqrt{3}}{2}t_2 \right) & \frac{1}{4}(t_{11} + 3t_{22}) & \pm \left(\frac{\sqrt{3}}{4}(t_{22} - t_{11}) \mp t_{12} \right) \\ \pm \frac{\sqrt{3}}{2}t_1 - \frac{1}{2}t_2 & \pm \left(\frac{\sqrt{3}}{4}(t_{22} - t_{11}) \pm t_{12} \right) & \frac{1}{4}(3t_{11} + t_{22}) \end{pmatrix} \quad (3)$$

The model we consider is obtained by adding intra-orbital on-site interactions to this model. Let $\mathbf{K} = \mathbf{K}_{\text{site}} \otimes \mathbf{K}_{\text{orb}}$ be the hopping matrix whose

hopping matrix in orbital space $\mathbf{t}(\mathbf{0}) \equiv \mathbf{t}^0 = \text{diag}(\varepsilon_1, \varepsilon_2, \varepsilon_2)$, while the NN hoppings are (see Fig.(1a))

$$\mathbf{t}(\mathbf{R}_{1,4}) \equiv \mathbf{t}^{1,4} = \begin{pmatrix} t_0 & \pm t_1 & t_2 \\ \mp t_1 & t_{11} & \pm t_{12} \\ t_2 & \mp t_{12} & t_{22} \end{pmatrix} \quad (2)$$

elements are the hoppings between the orbital α of site i and the orbital β of site j . Then, the intra-orbital Hubbard-like model corresponding to this minimal 3-band tight-binding model reads

$$\mathcal{H} = \overbrace{- \sum_{\substack{i,j \\ \alpha,\beta,\sigma}} K_{(i\alpha),(j\beta)} \left(c_{i,\alpha,\sigma}^\dagger c_{j,\beta,\sigma} + c_{j,\beta,\sigma}^\dagger c_{i,\alpha,\sigma} \right)}^{\mathcal{H}_K} + \underbrace{\frac{U}{2} \sum_{\substack{i,\alpha \\ \sigma \neq \sigma'}} n_{i\alpha,\sigma} n_{i\alpha,\sigma'}}_{\mathcal{H}_V} \quad (4)$$

2.2. Self-consistent solution in the GCE

Here, we start by showing how to obtain the solution of the mean field Hubbard Hamiltonian nu-

merically in an self-consistent manner, and then we generalize the procedure to treat the TMD nanoribbon.

The mean field Hubbard Hamiltonian reads

$$\mathcal{H}_{\text{MF}} = \mathcal{H}_\uparrow + \mathcal{H}_\downarrow + \mathcal{C}, \quad \mathcal{H}_\sigma = -t \sum_{\langle i,j \rangle} \left(c_{i,\sigma}^\dagger c_{j,\sigma} + c_{j,\sigma}^\dagger c_{i,\sigma} \right) + U \sum_i n_{i,\sigma} \langle n_{i,-\sigma} \rangle, \quad \mathcal{C} = -U \sum_i \langle n_{i,\uparrow} \rangle \langle n_{i,\downarrow} \rangle \quad (5)$$

We seek the most energetically favorable self-consistent solution iteratively¹: the up and down-spin electron densities are updated successively until convergence occurs.

Since the interacting problem is turned into a single particle problem, the solution basically consists of diagonalizing two $N \times N$ matrices, where N is the size of the system. By varying the $2N$ mean field parameters, which are essentially the average

local densities $\langle n_{i,\sigma} \rangle$, we can find the ground state, or other excited states, at the mean field level. The mean field approach has several advantages: the Hilbert space is reduced from exponential to linear in the system size, which allows the study of relatively large systems; we can do the computation in real space; we can arbitrarily change the system geometry (introducing OBC, defects, nonuniform hoppings); the model is flexible: tight-binding, and interaction terms are easily added to the Hamiltonian. However, $SU(2)$ symmetry is broken, and electron correlations are neglected. Only long range

¹One must pay attention so as not to get stuck in metastable states.

order is captured and its stability is often overestimated. While the mean field solution approaches the exact solution at weak coupling U , it can give only qualitative behavior at best, when U increases significantly.

The iterative method starts with the initialization of the mean field parameters. This initial condition cannot be completely arbitrary because it affects convergence. Typical choices are the random initial condition or the paramagnetic state. Then, we repeat the following steps until convergence.

First, we diagonalize \mathcal{H}_σ , obtaining the one-particle spectrum $\varepsilon_{\alpha,\sigma}$ and the corresponding eigenvectors.

$$\mathcal{H}_{\text{MF}} = \sum_{\alpha,\sigma} \varepsilon_{\alpha,\sigma} d_{\alpha,\sigma}^\dagger d_{\alpha,\sigma} + \mathcal{C}, \quad d_{\alpha,\sigma} = \sum_i Q_{\alpha i,\sigma}^* c_{i,\sigma} \quad (6)$$

Given a number of electrons per unit cell, n_e , we compute the chemical potential corresponding to that filling implicitly through

$$\frac{1}{N} \sum_{\alpha,\sigma} (e^{\beta(\varepsilon_{\alpha,\sigma} - \mu)} + 1)^{-1} = n_e$$

We use the bisection method.

Then, we recompute the mean field parameters, and check for convergence: at iteration I , $\langle n_{i,\sigma} \rangle_I \approx \langle n_{i,\sigma} \rangle_{I-1}$.

$$\langle n_{i,\sigma} \rangle = \sum_\alpha |Q_{\alpha i,\sigma}|^2 (1 + e^{\beta(\varepsilon_{\alpha,\sigma} - \mu)})^{-1} \quad (7)$$

Now, we discuss how to circumvent the convergence issues that may arise when applying the self-consistent procedure. First, there are many possible initial conditions, most notably: the random one, which is the most unbiased, but may be slow or not converge at all; the paramagnetic state $\langle n_{i,\sigma} \rangle = \text{const.}$, which, when combined with the annealing method we shall describe below, emulates the random initial condition; a specific state, such as the antiferromagnetic one, which is a biased choice, which limits the accessible part of parameter

$$\begin{aligned} \mathcal{H}_0 = & \sum_{m,n} \left(c_{m,n,\alpha}^\dagger t_{\alpha\beta}^0 c_{m,n,\beta} + \delta_{0,N_x} c_{m,n,\alpha}^\dagger t_{\alpha\beta}^1 c_{m+1,n,\beta} + \delta_{-\sqrt{3}/2,(N_y-1)\sqrt{3}/2} c_{m,n,\alpha}^\dagger t_{\alpha\beta}^4 c_{m-1,n,\beta} \right. \\ & + \delta_{0,N_m} \delta_{-1,(N_y-1)\sqrt{3}/2} c_{m+1/2,n-\sqrt{3}/2,\alpha}^\dagger t_{\alpha\beta}^2 c_{m,n,\beta} + \delta_{-1,(N_y-1)\sqrt{3}/2} c_{m-1/2,n-\sqrt{3}/2,\alpha}^\dagger t_{\alpha\beta}^3 c_{m,n,\beta} \\ & \left. + \delta_{N_y\sqrt{3}/2,0} c_{m+1/2,n+\sqrt{3}/2,\alpha}^\dagger t_{\alpha\beta}^6 c_{m,n,\beta} + \delta_{-1,N_x-1} \delta_{N_y\sqrt{3}/2,0} c_{m-1/2,n+\sqrt{3}/2,\alpha}^\dagger t_{\alpha\beta}^5 c_{m,n,\beta} \right) \end{aligned} \quad (10)$$

Fourier transforming along m : $c_{m,n,\alpha} = \frac{1}{\sqrt{N_x}} \sum_k e^{-ikm} c_{k,n,\alpha}$, with $k = \frac{2\pi}{N_x} \{-\frac{N_x}{2} + 1, -\frac{N_x}{2}, \dots, \frac{N_x}{2}\}$:

$$\begin{aligned} \mathcal{H}_0 = & \sum_{k,y} \left(c_{k,y,\alpha}^\dagger (t_{\alpha\beta}^0 + e^{ik} t_{\alpha\beta}^1 + e^{-ik} t_{\alpha\beta}^4) c_{k,y,\beta} + \delta_{-1,N_y-1} c_{k,y-1,\alpha}^\dagger (e^{ik/2} t_{\alpha\beta}^2 + e^{-ik/2} t_{\alpha\beta}^3) c_{k,y,\beta} \right. \\ & \left. + \delta_{N_y,0} c_{k,y,\alpha}^\dagger (e^{ik/2} t_{\alpha\beta}^6 + e^{-ik/2} t_{\alpha\beta}^5) c_{k,y+1,\beta} \right), \quad \text{with } y \text{ defined as in Fig.(4.1)} \end{aligned} \quad (11)$$

space, and potentially gives a misleading mean field solution, but can have good convergence properties.

In some cases, the symmetry of the system dramatically slows down convergence. By starting the procedure at a higher temperature than the desired one, we can improve convergence. The temperature is then gradually lowered until the desired one is achieved, and this procedure is applied at that temperature. There are a lot of possible such so called annealing schemes, namely keeping β fixed for some iterations and then adjusting it to the desired $\beta = \beta_0$, or smoothly reducing β until it reaches β_0 . A common convergence issue is the oscillation between two configurations $\langle n_{i,\sigma} \rangle_I \leftrightarrow \langle n_{i,\sigma} \rangle_{I+1}$. This is solved by averaging the values obtained at the current and previous iterations:

$$\langle n_{i,\sigma} \rangle_{I+1} \leftarrow \frac{1}{2} \langle n_{i,\sigma} \rangle_I + \frac{1}{2} \langle n_{i,\sigma} \rangle_{I+1}. \quad (8)$$

The weights attributed to each configuration can be also be different, or even vary with the iteration:

$$\langle n_{i,\sigma} \rangle_{I+1} \leftarrow P(I) \langle n_{i,\sigma} \rangle_I + (1 - P(I)) \langle n_{i,\sigma} \rangle_{I+1}, \quad (9)$$

if we make sure that $P(I) > \delta$, the latter being the convergence parameter.

Finally, the number of parameters may be reduced. This is done while taking into account the symmetry of the system. For example, one may take only the number of sublattices, say 2 for a square lattice with PBC. This corresponds to the uniform density ansatz $\langle n_{i,\sigma} \rangle = n_X = \frac{1}{N_X} \sum_{i \in X} \langle n_{i,\sigma} \rangle$ for all sites in the X sublattice. If this reduction is not done correctly, we will obtain biased self-consistent solutions that do not necessarily reflect the nature of the solution.

Since we consider PBCs along the x -direction for the nanoribbon, we can partially diagonalize the Hamiltonian analytically, reducing the size of the matrix to be diagonalized to $N_{\text{orb}} N_y \times N_{\text{orb}} N_y$, where N_y is the width of the ribbon, i.e. the number of MX_2 formula units. Consider the spinless 3-band tight binding model on the nanoribbon, with unit lattice constant.

leading to a tridiagonal block $3N_y \times 3N_y$ hopping matrix $\mathbf{H}(k)$ with three different types of matrix elements: $\mathbf{h}_1 = \mathbf{H}_{y,y}$, $\mathbf{h}_2 = \mathbf{H}_{y,y-1}$, $\mathbf{h}_2^\dagger = \mathbf{H}_{y,y+1}$.

$$[H_{(\alpha y)(\beta y')}(k)] = \begin{pmatrix} \mathbf{h}_1 & \mathbf{h}_2^\dagger & \\ \mathbf{h}_2 & \mathbf{h}_1 & \mathbf{h}_2^\dagger \\ & \mathbf{h}_2 & \mathbf{h}_1 & \ddots & \\ & & \ddots & \ddots & \mathbf{h}_2^\dagger \\ & & & \ddots & \mathbf{h}_2 \\ & & & & \mathbf{h}_2 & \mathbf{h}_1 \end{pmatrix}, \quad \mathbf{h}_1 = \begin{pmatrix} \varepsilon_1 + 2t_0 \cos k & 2it_1 \sin k & 2t_2 \cos k \\ -2it_1 \sin k & \varepsilon_2 + 2t_{11} \cos k & 2it_{12} \sin k \\ 2t_2 \cos k & -2it_{12} \sin k & \varepsilon_2 + 2t_{22} \cos k \end{pmatrix} \quad (12)$$

$$\mathbf{h}_2 = \begin{pmatrix} 2t_0 \cos(k/2) & i \sin(k/2) \left(t_1 - \sqrt{3}t_2 \right) & -\cos(k/2) \left(\sqrt{3}t_1 + t_2 \right) \\ -i \sin(k/2) \left(t_1 + \sqrt{3}t_2 \right) & \frac{1}{2} \cos(k/2) \left(t_{11} + 3t_{22} \right) & -i \sin(k/2) \left(\frac{\sqrt{3}}{2} (t_{11} - t_{22}) + 2t_{12} \right) \\ \cos(k/2) \left(\sqrt{3}t_1 - t_2 \right) & -i \sin(k/2) \left(\frac{\sqrt{3}}{2} (t_{11} - t_{22}) - 2t_{12} \right) & \frac{1}{2} \cos(k/2) \left(3t_{11} + t_{22} \right) \end{pmatrix}$$

In fact, by applying our mean field approach in real space to solve the 3-band model with Hubbard-type interactions, we obtain solutions that are independent of x (the longitudinal coordinate on the ribbon), which motivates us to reduce the number of MF parameters by choosing the translationally invariant ansatz introduced above. This is equivalent to taking $\langle n_{x,y,\alpha,\sigma} \rangle = \langle n_{y,\alpha,\sigma} \rangle \forall x$ ($6N_y$ parameters). By

$$\mathcal{H}_{\text{MF}} = \mathcal{H}_0 + \mathcal{H}_1 + \mathcal{C}, \text{ where } \mathcal{H}_1 = U \sum_{m,n,\alpha} \sum_{\sigma} n_{m,\alpha} \langle n_{m,-\sigma} \rangle, \quad \mathcal{C} = -U \sum_{m,n,\alpha} \langle n_{m,\uparrow} \rangle \langle n_{m,\downarrow} \rangle \quad (13)$$

$$\begin{aligned} \mathcal{H}_1 + \mathcal{C} &= \frac{U}{N_x^2} \sum_{\substack{n\alpha \\ k_1 k_2 \\ k_3 k_4}} \underbrace{\sum_m e^{i[(k_1+k_3)-(k_2+k_4)]m}}_{N_x \delta_{k_4, k_1+k_3-k_2}} \left(\underbrace{\sum_{\sigma} c_{k_1,n,\alpha}^\dagger c_{k_2,n,\alpha} \langle c_{k_3,n,\alpha}^\dagger c_{k_4,n,\alpha} \rangle}_{\delta_{k_3,k_4} \langle n_{k_3,-\sigma} \rangle} - \underbrace{\langle c_{k_1,n,\alpha}^\dagger c_{k_2,n,\alpha} \rangle}_{\delta_{k_1,k_2} \langle n_{k_2,\uparrow} \rangle} \underbrace{\langle c_{k_3,n,\alpha}^\dagger c_{k_4,n,\alpha} \rangle}_{\delta_{k_3,k_4} \langle n_{k_3,\downarrow} \rangle} \right) \\ &= \frac{U}{N_x} \sum_{\substack{n\alpha \\ k_2 k_3}} \left(\sum_{\sigma} n_{k_2,\sigma} \langle n_{k_3,-\sigma} \rangle - \langle n_{k_2,\uparrow} \rangle \langle n_{k_3,\downarrow} \rangle \right) \equiv U \sum_{k,\mu} \left(\sum_{\sigma} n_{k,\mu,\sigma} \langle n_{\mu,-\sigma} \rangle - \langle n_{\mu,\uparrow} \rangle \langle n_{\mu,\downarrow} \rangle \right) \end{aligned} \quad (14)$$

where we collapsed the indexes (n, α) into a single index μ . The self-consistent relation allowing us to compute the new MF parameters at each step emerges by diagonalizing \mathcal{H}_1 in the μ -subspace:

$$\begin{aligned} \langle n_{\mu,\sigma} \rangle &= \frac{1}{N_x} \sum_{q,\nu} |Q_{q\sigma\mu,\nu}|^2 \rho(\varepsilon_{q\nu\sigma}), \\ \text{where } d_{q,\sigma,\nu} &= \sum_{\nu} Q_{q\sigma\mu,\nu}^* c_{q,\sigma,\mu}, \\ \text{and } \mathcal{H}_{\text{MF}} &= \sum_{q,\nu,\sigma} \varepsilon_{q,\nu,\sigma} d_{q,\nu,\sigma}^\dagger d_{q,\nu,\sigma} + \mathcal{C} \end{aligned} \quad (15)$$

2.3. Auxiliary field Quantum Monte Carlo
This method is based on introducing an additional lattice field that mediates the electron-electron interaction. The interacting problem then becomes a

reducing the number of parameters, convergence is facilitated, which makes it more likely that, for example, the solution of Fig.(7) is robust, i.e. it does not correspond to a metastable. The mean field form of the interaction term with the reduced number of parameters changes, implying that the self-consistent relation of Eq.(7) from which the local densities are computed changes as well.

problem of independent fermions coupled to an external field, and the fermionic part of the partition function can be traced out explicitly, leaving the contribution of a *discrete*² classical field, \mathbf{h} . This contribution can be evaluated numerically by employing importance sampling over the field configurations. Auxiliary field QMC relies on a mapping to a so called “classical” system (in quotes because there may be no actual classical analogue):

$$Z = \text{Tr}[e^{-\beta \mathcal{H}}] = \sum_{\{\mathbf{h}\}} \sum_{\text{fermionic}} e^{-S} = \sum_c p(c), \quad (16)$$

²The introduced field is discrete (and *binary*) because each fermionic state can only have occupations $n = 0, 1$. Although, there is a finite number of field configurations, the number grows exponentially with the number of sites on the lattice.

but some of the “probabilities” $p(c)$ can actually be negative due to the antisymmetry of the many-electron wavefunction under electron exchange. Here, S is a fermion-field action that we shall write out explicitly later. For a fixed configuration of the \mathbf{h} field, we sum over the fermionic part exactly to obtain the weight of each configuration $p(c)$. The sum over \mathbf{h} is carried out stochastically. The negative weight problem can be circumvented when computing the average of an observable A :

$$\langle A \rangle = \frac{\sum_c A(c) |p(c)| \text{sign}[p(c)] / \sum_c |p(c)|}{\sum_c |p(c)| \text{sign}[p(c)] / \sum_c |p(c)|} \equiv \frac{\langle As \rangle_{|p|}}{\langle s \rangle_{|p|}}, \quad (17)$$

where $s(c) = \text{sign}[p(c)]$, and $|p(c)|$ corresponds to an auxiliary bosonic system (also coupled to the classical field) corresponding to the original fermionic system, and for which there is no sign problem.

The relative error $\Delta s / \langle s \rangle$ increases exponentially with the number of particles, with inverse temperature, and possibly with other parameters of the specific model to be studied [3, 4]. To see this, we start by noting that the average sign is the ratio between the partition functions of the fermionic ($Z = \sum_c p(c)$) and bosonic systems ($Z' = \sum_c |p(c)|$). In terms of the difference in free energy densities, $\langle s \rangle = Z/Z' = e^{-\beta N_p \Delta f}$, implying that for M samples, the error of the denominator of Eq. (17) becomes

$$\frac{\Delta s}{\langle s \rangle} = \frac{\sqrt{(\langle s^2 \rangle - \langle s \rangle^2)/M}}{\langle s \rangle} = \frac{\sqrt{1 - \langle s \rangle^2}}{\sqrt{M} \langle s \rangle} \propto \frac{e^{\beta N_p \Delta f}}{\sqrt{M}}, \quad (18)$$

and similarly for the numerator of Eq. (17).

For the sake of comparison, recall that mean field theory may be formulated by applying the Hubbard-Stratonovich (HS) transformation to transform an interacting problem into a one-body problem, and then apply the saddle-point approximation to solve the resulting integrals. In the Grand-canonical Ensemble (GCE), we take $\mathcal{H} \mapsto \mathcal{H} - \mu \mathcal{N}$, \mathcal{N} being the total particle number). The grand-partition function may be written in terms of a functional integral over a space-time dependent field of the exponential of a one-body action

$$Z = \text{Tr}[e^{-\beta \mathcal{H}}] = \int \mathcal{D}\mathbf{h} e^{-S(\mathbf{h})} \equiv \text{Tr}_{\mathbf{h}}[e^{-S(\mathbf{h})}], \quad (19)$$

which may be computed by Monte Carlo sampling. In mean field, we approximate the integral by replacing the functional integral by a constant times the exponential of the action - evaluated at the field \mathbf{h}^* , for which the action has a minimum: $\partial_{\mathbf{h}} S(\mathbf{h})|_{\mathbf{h}=\mathbf{h}^*} = 0$, and $\partial_{\mathbf{h}}^2 S(\mathbf{h})|_{\mathbf{h}=\mathbf{h}^*} > 0$. This approach depends on the HS decoupling that was used. In contrast, with the auxiliary field QMC

method, one computes the integral directly. Although it is more expensive in computing time ($\mathcal{O}(\beta N^3)$), it does not rely on any particular choice of the decoupling. Another obstacle of taking into account all the fluctuations around \mathbf{h}^* is the fermion sign problem. However, in certain cases, the symmetries of the model (like particle-hole) may be used to avoid it.

The Trotter-Suzuki decomposition leads to an approximate factorization of $e^{-\beta(\mathcal{H}_K + \mathcal{H}_V)}$ that is used to evaluate the partition function. Dividing the imaginary time interval $[0, \beta]$ into L equal subintervals of smaller width $\Delta\tau = \beta/L$, one obtains:

$$Z = \text{Tr} \left[\prod_{l=0}^{L-1} e^{-\Delta\tau \mathcal{H}^l} \right], \quad (20)$$

a form that is more amenable to computation. Actually, by writing the matrix elements of the projection operator \mathcal{P} as path-integrals (here, time-ordering is implicit [5]):

$$\begin{aligned} \langle \psi | e^{-\beta \mathcal{H}} | \psi' \rangle &= \sum_{|\psi_1\rangle, |\psi_2\rangle, \dots, |\psi_{L-1}\rangle} \langle \psi | e^{-\Delta\tau \mathcal{H}} | \psi_1 \rangle \\ &\quad \langle \psi_1 | e^{-\Delta\tau \mathcal{H}} | \psi_2 \rangle \dots \langle \psi_{L-1} | e^{-\Delta\tau \mathcal{H}} | \psi' \rangle, \end{aligned} \quad (21)$$

we see that it is the same as the partition function, if the paths are periodic in imaginary time:

$$\begin{aligned} Z &= \text{Tr}[e^{-\beta \mathcal{H}}] = \sum_{|\psi_0\rangle} \langle \psi_0 | e^{-\beta \mathcal{H}} | \psi_0 \rangle \\ &= \sum_{\{|\psi_l\rangle\}} \prod_{l=0}^{L-1} \langle \psi_l | e^{-\Delta\tau \mathcal{H}} | \psi_{l+1} \rangle = \text{Tr} \left[\prod_{l=0}^{L-1} e^{-\Delta\tau \mathcal{H}^l} \right], \end{aligned} \quad (22)$$

where we have $|\psi_L\rangle = |\psi_0\rangle$. We recover Eq.(20) by reorganizing the summations over $\{|\psi_l\rangle\}$, and using closure relations in the Hilbert space of each slice. Simply put, the “Trotter breakup” follows from truncating the inverse of the well known Baker-Campbell-Hausdorff formula, and keeping only the first order term in $\Delta\tau$.

The kinetic energy term is quadratic in the fermion operators, and spin-independent, meaning that it be separated into two spin components, independently of the time slice.

$$e^{-\Delta\tau \mathcal{H}_K} = e^{-\Delta\tau \mathcal{H}_{K\uparrow}} e^{-\Delta\tau \mathcal{H}_{K\downarrow}}, \quad (23)$$

where $\mathcal{H}_{K\sigma} = \mathbf{c}_\sigma^\dagger (-t_\sigma \mathbf{K}_\sigma - \mu_\sigma \mathbf{I}) \mathbf{c}_\sigma$.

The potential energy term, however, is quartic. Fortunately, it is possible to express it in quadratic form by introducing an extra degree of freedom, the so called *Hubbard-Stratonovich (HS) field* $\mathbf{h} \equiv (h_{l,i})_{i=0, l=0}^{N-1, L-1}$, in which each element is

essentially an Ising spin. At each slice, the interaction is eliminated by an N -dimensional HS field $\tilde{\mathbf{h}}$. We start by noting that $[n_{i,\sigma}, n_{j,\sigma'}] = 0 \forall i, j, \sigma, \sigma'$, so that in particle-hole symmetric-form³

$$e^{-\Delta\tau\mathcal{H}_V} = \prod_i e^{-U\Delta\tau(n_{i\uparrow}-1/2)(n_{i\downarrow}-1/2)} \quad (24)$$

The HS transformation is based on the well known identity $e^{\frac{a^2}{2}} = \frac{1}{\sqrt{2\pi}} \int_{-\infty}^{\infty} e^{-\frac{z^2}{2}-za} dz \forall a > 0$, which is also valid if a is an operator \mathcal{A} . Noting that $(n_{i\uparrow} - \frac{1}{2})(n_{i\downarrow} - \frac{1}{2}) = -\frac{1}{2}(n_{i\uparrow} - n_{i\downarrow})^2 + \frac{1}{4}$, we can recast the potential energy term as

$$\begin{aligned} e^{-\Delta\tau\mathcal{H}_V} &= \prod_i e^{\frac{U\Delta\tau}{2}(n_{i\uparrow}-n_{i\downarrow})^2} e^{-\frac{U\Delta\tau}{4}} = \left(\frac{\Delta\tau}{\pi}\right)^{N/2} \\ &\cdot e^{-\frac{NU\Delta\tau}{4}} \int_{-\infty}^{\infty} \prod_i d\tilde{h}_i e^{-\Delta\tau[\tilde{h}_i^2 + \sqrt{2U}(n_{i\uparrow}-n_{i\downarrow})\tilde{h}_i]}, \end{aligned} \quad (25)$$

so that in the $\tau \rightarrow 0$ limit, the partition function becomes

$$\begin{aligned} Z &\propto \int \mathcal{D}\tilde{\mathbf{h}}(\tau) e^{-\int_0^\beta d\tau \tilde{\mathbf{h}}^2(\tau)} \\ &\cdot \text{Tr} \left[\mathcal{T}_\tau e^{-\int_0^\beta d\tau [\mathcal{H}_K(\tau) + \sqrt{2U}(\mathbf{n}_{\uparrow}(\tau) - \mathbf{n}_{\downarrow}(\tau)) \cdot \tilde{\mathbf{h}}(\tau)]} \right], \end{aligned} \quad (26)$$

representing a system of noninteracting fermions coupled via spin S_i^z to an external fluctuating real field.

The fact that $n_{i,\sigma}$ can only take on two possible values suggests an analogous transformation in which the fluctuating field can only take on two possible values. An Ising spin will prove sufficient to eliminate the direct electron-electron interaction. The discrete HS transformation for $U > 0$ allows us to recast Eq.(24) in terms of the local spin, a non-interacting quadratic term $n_{i\uparrow} - n_{i\downarrow}$ (at each imaginary-time slice, since the operators live on the Hilbert space of that specific slice). Let $c_U = \frac{1}{2}e^{-\frac{U\Delta\tau}{4}}$ and $\nu = \text{arcosh}(e^{\frac{U\Delta\tau}{2}})$. Then, the sought transformation reads

$$e^{-U\Delta\tau(n_{i\uparrow}-1/2)(n_{i\downarrow}-1/2)} = c_U \sum_{\tilde{h}_i=\pm 1} e^{\nu\tilde{h}_i(n_{i\uparrow}-n_{i\downarrow})} \quad (27)$$

For each imaginary time slice l , we may define a HS-field $\tilde{\mathbf{h}}_l$, which specifies \mathbf{V}_l and $\mathcal{H}_{V_\sigma}^l$. The Hamiltonian acquires a “fictitious” imaginary-time dependence that enforces (imaginary-)time ordering, and independent Hilbert spaces at each slice.

³The particular model in which we are interested does not have particle-hole symmetry (PHS), but the HS transformation is done in PHS-form for convenience when we simulate PHS models. One simply has to remember that the PH transformation shifts the chemical potential by $\frac{U}{2}$.

After some algebra,

$$Z = (c_U)^{NL} \text{Tr}_{\mathbf{h}} \text{Tr} \left[\prod_{l=0}^{L-1} \prod_{\sigma} \underbrace{e^{-\Delta\tau\mathcal{H}_{K\sigma}} e^{\mathcal{H}_{V_\sigma}^l}}_{\mathbf{B}_{l,\sigma}(\tilde{\mathbf{h}}_l)} \right], \quad (28)$$

where all operators are now quadratic in the fermion operators:

$$\mathcal{H}_{K\sigma} = \mathbf{c}_\sigma^\dagger (-t_\sigma \mathbf{K}_\sigma - \mu_\sigma \mathbf{I}) \mathbf{c}_\sigma \quad \mathcal{H}_{V_\sigma}^l = \sigma\nu \mathbf{c}_\sigma^\dagger \mathbf{V}_l(\tilde{\mathbf{h}}_l) \mathbf{c}_\sigma \quad (29)$$

for $\sigma = \pm 1$ and $\mathbf{V}_l(\tilde{\mathbf{h}}_l) = \text{diag}(h_{l,0}, h_{l,1}, \dots, h_{l,N-1})$. The problem of computing the partition function has been reduced to computing the trace of a product of exponentials of quadratic forms. Thus, we may still rewrite equation (28) by making use of the following identity. Let \mathcal{H}_l be quadratic forms of the fermion operators: $\mathcal{H}_l = c_i^\dagger(\mathbf{H}_l)_{ij} c_j$, where the summation is implied, and where \mathbf{H}_l are real matrices. Then, the following identity holds

$$\text{Tr} [e^{-\mathcal{H}_1} e^{-\mathcal{H}_2} \dots e^{-\mathcal{H}_L}] = \det(\mathbf{I} + e^{-\mathbf{H}_L} \dots e^{-\mathbf{H}_1}) \quad (30)$$

Since we mapped our interacting quantum problem to a higher dimensional “classical” problem of higher dimension, we can use the Metropolis algorithm with single spin flip dynamics to generate samples from the distribution of the classical field $p(c) \propto \prod_{\sigma} \det[\mathbf{I} + \prod_l \mathbf{B}_{l,\sigma}(\tilde{\mathbf{h}}_l)]$. The determinants are not computed explicitly. Instead they are updated at each step by use of the Sherman-Morrison-Woodbury formula, in a procedure that scales as $\mathcal{O}(N^2)$. The single-particles Green’s functions of the free-fermion problem we obtain after using the HS transformation are represented by the matrices $\mathbf{G}^\sigma = (\mathbf{I} + \prod_l \mathbf{B}_{l,\sigma}(\tilde{\mathbf{h}}_l))^{-1}$. By using Wick’s theorem, we can write any quantum observable in terms of combinations of matrix elements of the Green’s matrices \mathbf{G}^σ . We measure the relevant observables for our problem during the Monte Carlo sampling, for example: the electron density $\rho = \frac{1}{N} \sum_{i,\sigma} \langle n_{i,\sigma} \rangle$, related to the filling; the (equal-time) spin-spin correlation $\langle S_i^z S_j^z \rangle$, where $S_i^z = n_{i\uparrow} - n_{i\downarrow}$, whose Fourier transform gives the magnetic structure factor $S(\mathbf{q})$; the time-displaced spin-spin correlator $\langle S_i^z(\tau) S_j^z(0) \rangle$, which gives us the (momentum-dependent) susceptibility

$$\chi(\mathbf{q}) = \frac{1}{N} \sum_{i,j} e^{i\mathbf{q} \cdot (\mathbf{R}_i - \mathbf{R}_j)} \int_0^\beta d\tau \langle S_i^z(\tau) S_j^z(0) \rangle \quad (31)$$

3. Results

3.1. Stabilization

Determinant Quantum Monte Carlo suffers from low temperature and large size numerical instabilities. These arise because the information about the

quantum states we seek is encoded in the differences between matrix elements of largely different magnitude contained in the elements of the \mathbf{B} -matrices of Eq.(28). It is outside of the scope of this document to describe the stabilization procedure (it is done in the thesis). In short, we find the energy scales that gives us the relevant information we seek via a QR decomposition with partial pivoting (following [6]), and then we cut off the irrelevant scales that destabilize the matrix products we need to compute, using a matrix \mathbf{D}' (the notation becomes clear in the thesis).

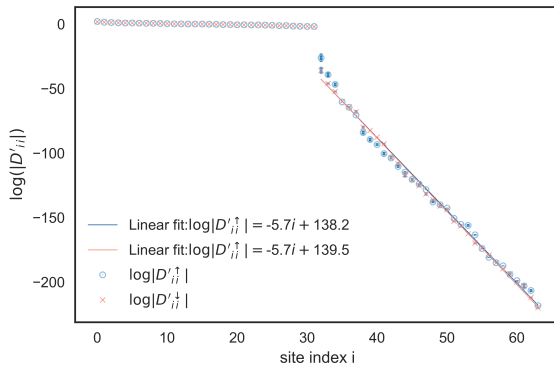


Figure 3: The matrix \mathbf{D}' (standard notation used in the thesis) displays the scales spanned by the stably multiplied \mathbf{B} -matrices (in this case for $\beta = 20t$, $U = 8t$, on a 64-site 1D chain with periodic boundary conditions).

3.2. Benchmarks

Our comparison with the auxiliary field QMC results of QUEST for a 64-site 1D chain with periodic boundary conditions with $U = 4t$, and $\beta = 25t$, shows remarkable agreement, namely in the magnetic structure factor.

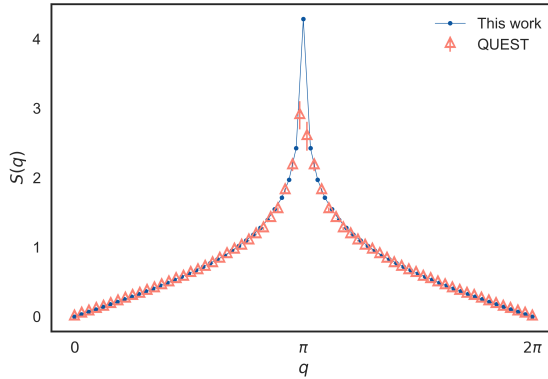


Figure 4: Comparison between our measurement magnetic structure factor and the result obtained when we ran QUEST

Another benchmark is the result that we obtain for the magnetic ordering in a strained graphene

nanoribbon, reproducing the results of a recent paper [7]. The prediction of our mean field calculation for a strained graphene nanoribbon (with hoppings reduced along its longitudinal x direction $t \mapsto t - \Delta$, $\Delta = 0.3t$) is that the spins along the rows of the ribbon have uniform correlation. In fact, we can see that mean field overestimates long range ordering, and they follow instead the symmetric profile of Fig.(5), a behavior typical of this type of graphene-based system [8, 9]. This result expands on the study carried out in [7].

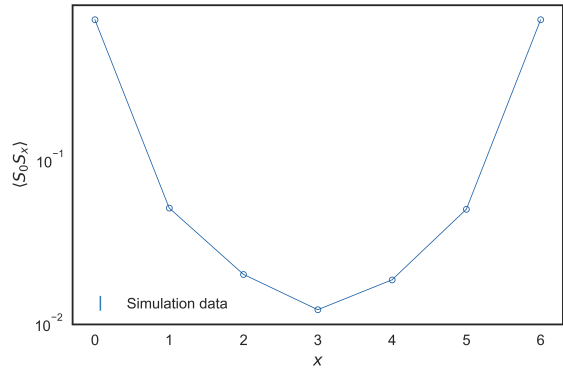


Figure 5: Profile of the spin-spin correlations along the edge for a 6×6 strained graphene nanoribbon at $\beta = 16$, $U = 3t$, $\Delta = 0.3$.

By computing the susceptibility on the edge (restricting the sum in Eq.(31) to sites on the edge) for one of the sublattices, we are to find the critical temperature for the transition to the ordered state for $U = 3t$, $T_c = (0.017 \pm 0.003)t$. This is done by fitting the results for the susceptibility obtained for our simulations run at different temperatures to the Curie Law $\chi \propto (T - T_c)^{-1}$ (see Fig.(6)). Repeating the procedure for varying temperature, and on-site interaction, we would be able to draw a complete phase diagram.

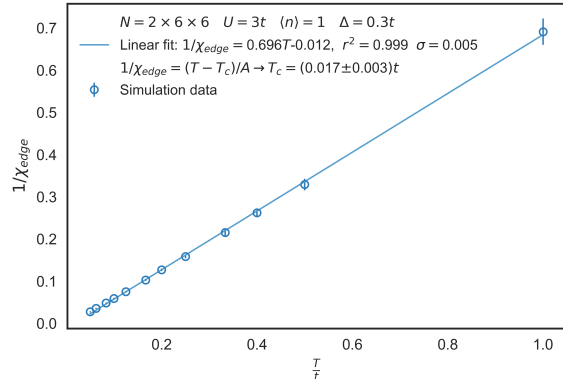


Figure 6: Fit of χ_{edge} to Curie's Law.

3.3. Mean field

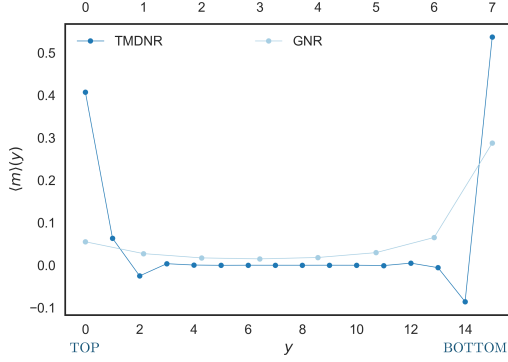


Figure 7: Spin density profile along the ribbon's transverse direction $\langle m \rangle(y)$ for the Hubbard model at half filling ($\langle n \rangle = 1$) for a 16×8 graphene nanoribbon (GNR) at $U = 1.2t$ (left) and a TMDNR with $N_y = 16$ at $U = 20|t_0|$, and electron density $\langle n \rangle = 0.66$, the filling that corresponds to charge neutrality.

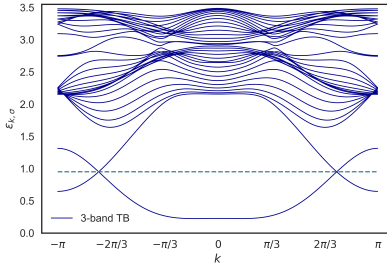


Figure 8: Comparison with QUEST

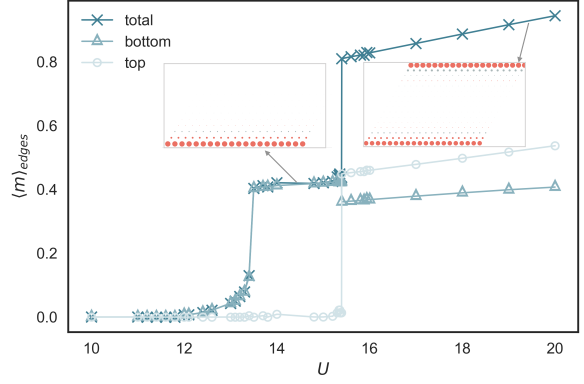


Figure 10: Mean field phase diagram at zero temperature. Zoom-in of the first phase transition.

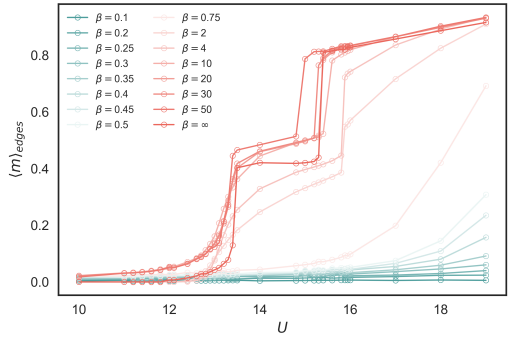


Figure 11: $T = 0$ mean field band structure for a TMD nanoribbon of width $N_y = 16$ in the ordered phase ($U = 20|t_0|$).

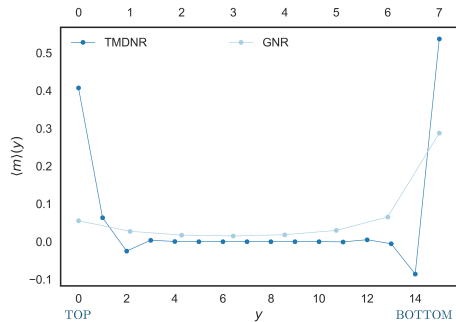


Figure 9: Comparison with QUEST

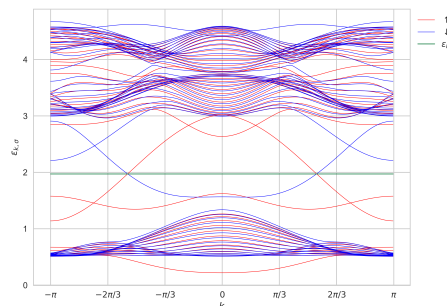


Figure 12: Comparison with QUEST

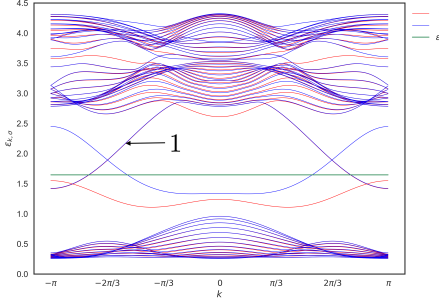


Figure 13: Comparison with QUEST

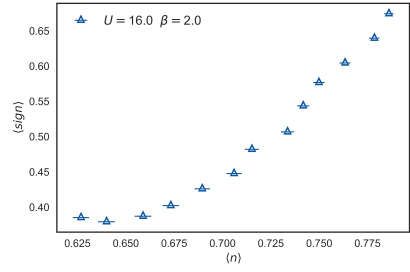


Figure 17: Comparison with QUEST

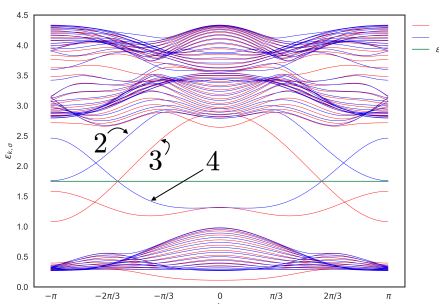


Figure 14: Comparison with QUEST

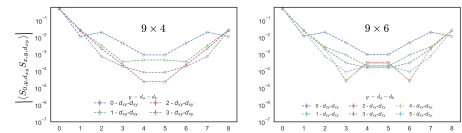


Figure 18: Comparison with QUEST

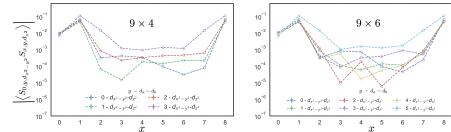


Figure 19: Comparison with QUEST

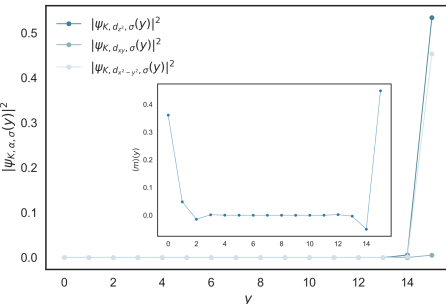


Figure 15: Comparison with QUEST

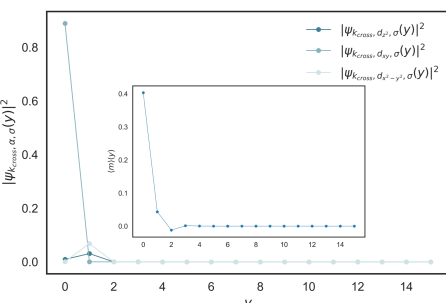


Figure 16: Comparison with QUEST

4. Conclusions

Conclusions, future work and some final remarks...

Acknowledgements

The author would like to thank ...

References

- Novoselov, K. S. *et al.* Electric Field Effect in Atomically Thin Carbon Films. *Science* **306**, 666–669. ISSN: 0036-8075, 1095-9203 (Oct. 22, 2004).
- Liu, G.-B., Shan, W.-Y., Yao, Y., Yao, W. & Xiao, D. Three-band tight-binding model for monolayers of group-VIB transition metal dichalcogenides. *Physical Review B* **88**, 085433 (Aug. 26, 2013).
- Troyer, M. & Wiese, U.-J. Computational Complexity and Fundamental Limitations to Fermionic Quantum Monte Carlo Simulations. *Physical Review Letters* **94**, 170201 (May 4, 2005).
- Bai, Z., Chen, W., Scalettar, R. & Yamazaki, I. in Hou, T. Y., Liu, C. & Liu, J.-G. *Series in Contemporary Applied Mathematics 1–110* (CO-PUBLISHED WITH HIGHER EDUCATION PRESS, June 2009). ISBN: 978-981-4273-25-1 978-981-4273-26-8. doi:10 . 1142 / 9789814273268 _0001. http://www.worldscientific.com/doi/abs/10 . 1142 / 9789814273268_0001 (2018).
- Hirsch, J. Discrete Hubbard-Stratonovich transformation for fermion lattice models. *Physical Review B* **28**, 4059–4061 (June 16, 1983).
- Bai, Z., Lee, C., Li, R.-C. & Xu, S. Stable solutions of linear systems involving long chain of matrix multiplications. *Linear Algebra and its Applications. Special Issue: Dedication to Pete Stewart on the occasion of his 70th birthday* **435**, 659–673. ISSN: 0024-3795 (Aug. 1, 2011).
- Yang, G., Li, B., Zhang, W., Ye, M. & Ma, T. Strain-tuning of edge magnetism in zigzag graphene nanoribbons. *Journal of Physics: Condensed Matter* **29**, 365601. ISSN: 0953-8984 (2017).

8. Feldner, H. *et al.* Dynamical Signatures of Edge-State Magnetism on Graphene Nanoribbons. *Physical Review Letters* **106**, 226401 (May 31, 2011).
9. Raczkowski, M. & Assaad, F. F. Interplay between the edge-state magnetism and long-range Coulomb interaction in zigzag graphene nanoribbons: Quantum Monte Carlo study. *Physical Review B* **96**, 115155 (Sept. 26, 2017).